

A new method to calculate broadband dielectric spectra of solvents from molecular dynamics simulations demonstrated with polarizable force fields

Cite as: *J. Chem. Phys.* **161**, 064306 (2024); doi: [10.1063/5.0217883](https://doi.org/10.1063/5.0217883)

Submitted: 7 May 2024 • Accepted: 26 July 2024 •

Published Online: 12 August 2024

Rebecca A. Bone,^{1,2}  Moses K. J. Chung,³  Jay W. Ponder,³  Demian Riccardi,⁴  Chris Muzny,⁴ 
Ravishankar Sundararaman,⁵  and Kathleen Schwarz^{2,a)} 

AFFILIATIONS

¹Theiss Research, P.O. Box 127, La Jolla, California 92038, USA

²Material Measurement Laboratory, National Institute of Standards and Technology, 100 Bureau Dr., Gaithersburg, Maryland 20899, USA

³Department of Chemistry, Washington University in St. Louis, St. Louis, Missouri 63130, USA

⁴Material Measurement Laboratory, National Institute of Standards and Technology, 325 Broadway, Boulder, Colorado 80305, USA

⁵Department of Materials Science and Engineering, Rensselaer Polytechnic Institute, 110 8th St., Troy, New York 12180, USA

Note: This paper is part of the JCP Special Topic on Molecular Dynamics, Methods and Applications 60 Years After Rahman.

^{a)}Author to whom correspondence should be addressed: kas4@nist.gov

ABSTRACT

Simulating the dielectric spectra of solvents requires the nuanced definition of inter- and intra-molecular forces. Non-polarizable force fields, while thoroughly benchmarked for dielectric applications, do not capture all the spectral features of solvents, such as water. Conversely, polarizable force fields have been largely untested in the context of dielectric spectroscopy but include charge and dipole fluctuations that contribute to intermolecular interactions. We benchmark non-polarizable force fields and the polarizable force fields AMOEBA03 and HIPPO for liquid water and find that the polarizable force fields can capture all the experimentally observed spectral features with varying degrees of accuracy. However, the non-polarizable force fields miss at least one peak. To diagnose this deficiency, we decompose the liquid water spectra from polarizable force fields at multiple temperatures into static and induced dipole contributions and find that the peak originates from induced dipole contributions. Broadening our inquiry to other solvents parameterized with the AMOEBA09 force field, we demonstrate good agreement between the experimental and simulated dielectric spectra of methanol and formamide. To produce these spectra, we develop a new computational approach to calculate the dielectric spectrum via the fluctuation dissipation theorem. This method minimizes the error in both the low and high frequency portions of the spectrum, improving the overall accuracy of the simulated spectrum and broadening the computed frequency range.

Published by AIP Publishing. <https://doi.org/10.1063/5.0217883>

INTRODUCTION

Dielectric spectroscopy captures a wide range of inter- and intra-molecular interactions, creating challenges for both theory and experiment. The frequency range of interest often spans six orders of magnitude, reflecting contributions ranging from collective molecular rotations to bond vibrations and angle bends.¹ Thus, multiple

experimental techniques spanning different frequency ranges^{2–5} are needed. Computational methods face a similar challenge. They must accurately represent both the intramolecular and intermolecular interactions to capture the low and high frequency portions of the dielectric spectrum.

Dielectric spectra are typically simulated using classical molecular dynamics (MD).^{6–8} In classical MD, a force field—the definition

of the potentials that create forces between the atoms in the simulation—can be polarizable or non-polarizable. Non-polarizable force fields can have combinations of point charges, dipoles, and quadrupoles on atoms in the simulation, but those multipoles are fixed in time throughout the simulation.^{9–13} Conversely, polarizable force fields can allow for induced charge, dipole effects,^{14–18} intermolecular charge transfer, and charge penetration.^{19–22} The calculation of such effects makes polarizable force fields more computationally expensive than their non-polarizable counterparts but still significantly less expensive than *ab initio* molecular dynamics (AIMD) methods.

Non-polarizable force fields have been tested extensively for their performance in capturing the static dielectric constant of various materials and, to a lesser extent, their dielectric spectra.^{23–30} However, these force fields cannot capture charge transfer effects, which are crucial in the nuanced representation of hydrogen bonding, as any multipoles are static in simulations. In contrast, AIMD, plus the inclusion of nuclear quantum effects for high-frequency peaks,³¹ has the potential to capture all the experimentally observed peaks in the dielectric spectrum of water.³² AIMD simulations of solvents with sufficient statistics to access dielectric properties below the Debye peak^{33,34} (for water, $\tau_D = 9$ ps) are not readily accessible. In practice, density functional theory functionals can dramatically overestimate the static dielectric constant.^{35,36} Machine learning methods of generating force fields are less expensive than AIMD methods but are not yet reliable for predicting the charges and dipoles necessary for simulating dielectric spectra.³⁷ In addition, these force fields are a significant challenge to parameterize for arbitrary solutions beyond a neat solvent.³⁸ Polarizable force fields have neither of these limitations, holding great promise due to their favorable balance between accuracy and computational efficiency.

The usual method of calculating dielectric spectra from these simulations is the fluctuation dissipation theorem (FDT).³⁹ In this method, a trajectory of an ensemble of molecules is simulated at equilibrium and the polarization is extracted. The susceptibility can be evaluated from the autocorrelation between the dipole moments of the total simulation at different times.⁴⁰ However, this only does well at capturing the low frequency portion of the dielectric spectrum. Conversely, one can take the Fourier transform of the dipole moments to access the spectrum. This is most effective at high frequencies.³²

Here, we demonstrate a method of computing an accurate dielectric spectrum over six decades of frequency using a single molecular dynamics simulation. We generate a spectrum for water from a combination of the autocorrelation and direct FDT methods, using estimates of the errors to determine the most accurate method at each frequency. Furthermore, by combining this method with polarizable force fields, we are able to split the contributions to the total dielectric spectrum into static and induced multipolar components. This allows us to decompose the spectrum and analyze the source of each peak. Benchmarking polarizable force fields against traditional non-polarizable force fields for water, we find that unlike non-polarizable force fields, polarizable force fields have the potential to capture all the peaks in the water spectrum. We then analyze the decomposed water spectrum at temperatures ranging from 275 to 350 K. Finally, we demonstrate the good agreement between the experiment and simulated spectra for two additional solvents. This illustrates the broad applicability of the AMOEBA polarizable force

field coupled with this method to capture solvent dynamics across a wide frequency range.

SIMULATION DETAILS

Note: certain software is identified in this paper to foster understanding. Such identification does not imply recommendation or endorsement by the National Institute of Standards and Technology, nor does it imply that the software identified is necessarily the best available for the purpose.

SPC/E and SPC/Fw (non-polarizable)

We benchmark two non-polarizable force fields for water: the simple point charge-extended (SPC/E) force field and the simple point charge-flexible (SPC/Fw) force field. For our SPC/E and SPC/Fw simulations,^{11,13,28} we constructed a simulation box of 500 molecules of water with packmol.⁴¹ We equilibrated the box for 5 ns in the NPT ensemble with periodic boundary conditions in the Large-scale Atomic/Molecular Massively Parallel Simulator (LAMMPS). Then, we simulated equilibrium dynamics in the NVT ensemble for 20 ns. We used the Nosé–Hoover thermostat and barostat with a temperature of 300 K and a pressure of 1 atm. We used the Verlet integration algorithm with a time step of 1 fs after confirming no substantive change in spectral output for both the force fields with time steps down to 0.1 fs and up to 2 fs. A cutoff distance of 12.0 Å was used for intermolecular interactions. Particle-particle particle-mesh (pppm) was used for Ewald summation.

The point charge on each atom in the SPC family of force fields is time-invariant. There are no higher order multipoles. Thus, the polarization is determined from the charge q and position (x, y, z) of the N atoms in the simulation,

$$P_y(t) = \sum_i^N q_i y_i(t), \quad (1)$$

for each dimension $y \in [x, y, z]$ of the simulation.

AMOEBA03, AMOEBA09, and HIPPO (polarizable)

We benchmarked two polarizable water models: the Atomic Multipole Optimized Energetics for Biomolecular Applications (AMOEBA03) water model and the Hydrogen-like Intermolecular Polarizable Potential (HIPPO) force field.^{14,15,19} The HIPPO force field extends the AMOEBA03 water model to include charge transfer energetics in addition to the various static and time-variant multipoles of AMOEBA03. We used the AMOEBA09 model for our simulations of formamide and methanol.¹⁵ For our AMOEBA03, AMOEBA09, and HIPPO simulations, we constructed a simulation box consisting of 500 molecules in an initial configuration generated by packmol.⁴¹ We equilibrated the simulation box for 5 ns in the NPT ensemble and then ran dynamics in the NVT ensemble for 10 ns for water, 20 ns for formamide, and 50 ns for methanol, both in Tinker.^{42,43} We used the Nosé–Hoover thermostat and barostat with temperatures of 275, 300, 325, and 350 K and a pressure of 1 atm. We used the Verlet integration algorithm with a time step of 1 fs after confirming that time steps down to 0.05 fs offered no substantive change to the spectral output. We included long-range electrostatics contributions in our periodic simulations using a standard Ewald

summation.¹⁴ We used a cutoff distance for long-distance van der Waals type interactions of 10 Å and an Ewald cutoff distance of 7 Å. Multipole analysis was performed in Tinker using the ANALYZE program following the dynamics simulation.

The polarization of the simulation box in AMOEBA03 and HIPPO simulations is determined from the combination of the time-invariant point-dipoles (as with the SPC family), the time-invariant (static) atomic dipoles μ^{sta} , and the time-variant (induced) atomic dipoles μ^{ind} ,

$$P_y(t) = \sum_i^N [q_i \gamma_i(t) + \mu_y^{sta} + \mu_y^{ind}(t)]. \quad (2)$$

The induced dipole moment is calculated for each time step in both AMOEBA03 and HIPPO.^{14,15,19} An induced dipoles print-out was added to the Tinker package to separate the induced and static dipole moment components.

FLUCTUATION DISSIPATION THEOREM

We extract the frequency-dependent imaginary susceptibility $\mathcal{I}m[\chi(\omega)]$ from the time series $\mathbf{P}(t)$ of the total dipole moment in the unit cell in two different ways detailed in the following. (Note that \mathbf{P} is the total system polarization and not the polarization density.) We then combine these results to optimize the accuracy based on the data for each frequency. We subsequently compute $\mathcal{R}e[\chi(\omega)]$ using the Kramers–Kronig relation.

Autocorrelation

First, we compute the autocorrelation of the total dipole moment,

$$\langle \mathbf{P}(0)\mathbf{P}(t) \rangle = \sum_i w_i \mathbf{P}(i)\mathbf{P}(i+t). \quad (3)$$

The weights w_i correspond to randomly sampling each possible start time i with replacement.

We then normalize the resulting autocorrelation to obtain $\sum_j w_j = 1$. For each such sampling, we compute the imaginary susceptibility,

$$\mathcal{I}m[\chi(\omega)] = \frac{\omega}{3Vk_B T \epsilon_0} \int_0^\infty dt \cos(\omega t) \langle \mathbf{P}(0)\mathbf{P}(t) \rangle, \quad (4)$$

where V is the volume of the simulation cell and ϵ_0 is the permittivity of free space. We repeat this analysis n_{repeat} times (specified by the variable n_{repeat} in our code; see the [supplementary material](#)) with different random weights and then compute the mean and standard deviation to obtain $\chi(\omega)$ with an error estimate.

This autocorrelation approach is similar to that of Ref. 44, except that we introduce error estimation to combine the results with a second approach that we detail in the following. In addition, we remove empirical fixes used by Ref. 44, such as setting $\langle \mathbf{P}(0)\mathbf{P}(t) \rangle = 0$ after it first crosses zero. The previously problematic regions are automatically addressed in our method when we combine the results of both approaches using error analysis.

Fourier transform

For our second approach, we apply the Wiener–Khinchin theorem to compute the imaginary susceptibility directly from the Fourier transform of the dipole time series, following the logic in Ref. 32. We perform this computation using a Gaussian window function,

$$\mathcal{I}m[\chi(\omega)] = \frac{\omega}{6Vk_B T \epsilon_0 \sigma \sqrt{\pi}} \cdot \left| \int_{t_0-n\sigma}^{t_0+n\sigma} dt \exp\left(-i\omega t - \frac{(t-t_0)^2}{2\sigma^2}\right) \mathbf{P}(t) \right|^2. \quad (5)$$

Here, for each ω , we pick the window size $\sigma = 1/(2\delta\omega)$, the uncertainty limit for time and frequency resolution in Fourier transforms, where $\delta\omega$ is the desired resolution in frequency. We set $\delta\omega$ to the spacing between ω on the logarithmic grid on which we generate the results. We repeat this calculation for window center t_0 spaced evenly by 2σ throughout the total time t_{max} of the trajectory. The Gaussian window width extends $n\sigma$ with $n = 3$ on either side of t_0 , such that its weight becomes negligible. This leads to $\lfloor t_{\text{max}}/(2\sigma) \rfloor - 2$ independent windows for which we apply Eq. (5). From these estimates of $\mathcal{I}m[\chi(\omega)]$ for each ω , we calculate the mean and standard errors.

Combination and error analysis

Finally, we combine the two estimates of $\mathcal{I}m[\chi(\omega)]$ above at each frequency, with μ and σ denoting the mean and standard errors, respectively, as

$$\mu_{\text{net}} = \frac{\sum_j \mu_j \sigma_j^{-2}}{\sum_j \sigma_j^{-2}}, \quad \text{and} \quad \sigma_{\text{net}} = \left(\sum_j \sigma_j^{-2} \right)^{-1/2}, \quad (6)$$

where $j \in \{\text{autocorrelation, Fourier}\}$, assuming a normal distribution for the uncertainty. Fig. 2S ([supplementary material](#)) shows the individual estimates with error bands for the two methods and the combined result for a short single trajectory of SPC/E MD as an example. It should be noted that the autocorrelation estimate is accurate at low frequencies and becomes increasingly inaccurate with increasing frequency. In contrast, the Fourier method has few windows and large errors at low frequencies and becomes increasingly accurate (error band vanishes on plot) with increasing frequency due to an increasing number of narrower time windows that can be used for analysis. Together, the combined result achieves excellent accuracy across the entire frequency range with relatively short trajectories, allowing us to perform the analysis with relatively expensive interatomic potential models. We also calculate the dielectric constant from these simulations using the equation,

$$\epsilon_s = \epsilon_\infty + \sum_{\gamma=x,y,z} \frac{\text{var}(P_\gamma)}{3Vk_B T \epsilon_0}, \quad (7)$$

where ϵ_∞ is the high frequency dielectric constant and $\text{var}(P_\gamma)$ denotes the variance of the polarization along the γ direction.

RESULTS AND DISCUSSION

Experimental and computational water spectra

In order to compare the spectra obtained from polarizable and non-polarizable force fields, we have aggregated several dielectric spectra of water from the literature^{45–54} to span the entire frequency range of interest (Fig. 1-gray). The low-frequency dielectric constant is ~ 78 . The imaginary portion of the spectrum shows six peaks corresponding to six relaxation processes. The mechanisms of these relaxation processes are commonly identified as: 1- collective reorientation,⁵⁵ 2- hydrogen bond translation or stretching,^{56,57} 3- libration,⁵⁷ 4- angle bending,⁵⁷ 5- intramolecular asymmetric O–H bond stretch,⁵⁷ and 6- intramolecular symmetric O–H bond stretch.⁵⁷ The dielectric magnitude and Debye relaxation constant of the peaks associated with these relaxation processes are provided in the [supplementary material](#)- Tables IS and IIS

To demonstrate the importance of polarizable force fields, we simulated two commonly used non-polarizable force fields for water: SPC/E and SPC/Fw. The dielectric spectra from water simulations using SPC/E and SPC/Fw are shown in Fig. 1(a). These results agree with the previously reported spectra.^{18,37} Both of these non-polarizable force fields get the time constant and magnitude of the Debye peak and the libration approximately correct. The rigid SPC/E model captures no other peaks in the spectrum, as expected. The flexible SPC/Fw model captures some of the high-frequency peaks, although their magnitudes and locations are incorrect. Neither of these models captures peak 2.

In contrast to non-polarizable models, both of the polarizable force fields capture all six of the expected peaks [Fig. 1(b)]. The dielectric constant of water is 89.4 ± 2.6 from the AMOEBA03 simulations but is better reproduced with the HIPPO force field, 77.7 ± 4.3 . These agree with the previously reported values.^{58,59} HIPPO performs better at capturing the dielectric constant of water, but notably does worse than AMOEBA03 at capturing all but the low frequency peak of the water spectrum.

We note that the static dielectric constant is known to be a difficult-to-converge quantity,³⁶ requiring long simulation times to adequately sample it. However, the behavior of the autocorrelation of the polarization for the imaginary spectrum converges much faster with increasing simulation time than the variance of the polarization. This is expected because the imaginary part of the spectrum

is constrained to converge to zero at low frequency [Eq. (4)], accumulating less error than the real part, which converges to ϵ_s . Our calculation of ϵ_s from four simulations, each 50 ns in length, has a greater error associated with it (see the [supplementary material Fig. 4](#)) than the imaginary component of the dielectric spectrum that we calculate with our method using only 10 ns [Fig. 1(b)]. Indeed, the imaginary component of the dielectric spectrum is largely unchanged in features using only 300 ps of simulation time (see the [supplementary material Fig. 1](#)), compared to a minimum of 10 ns of simulation time required for ϵ_s fluctuations to die down (see [supplementary material Fig. 4](#)).

Decomposition of computational spectra

Because we are using polarizable force fields, we can separate the contributions to the dielectric spectrum into the polarization contributions from the induced dipoles and static multipoles. In AMOEBA03, the total polarization has three terms: the static charge, the static dipole moment, and the induced dipole moment. We calculated the spectral components arising from the static and induced components of the total polarization (Fig. 2). We then analyze each peak to determine which spectral components contribute to it.

The static charge, static dipole, and induced dipole all contribute to the Debye peak (peak 1), although the contribution from

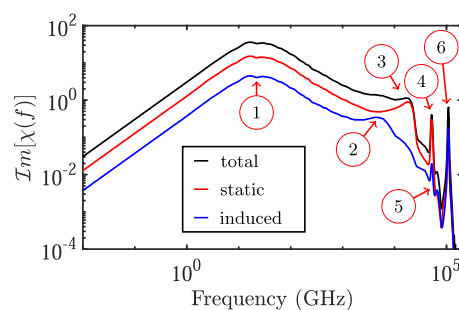


FIG. 2. Total dielectric spectrum (black) of water using the AMOEBA water model and dissected into contributions from induced (red) and static (blue) multipolar contributions (induced-static cross term not shown; see the [supplementary material](#)) at 300 K.

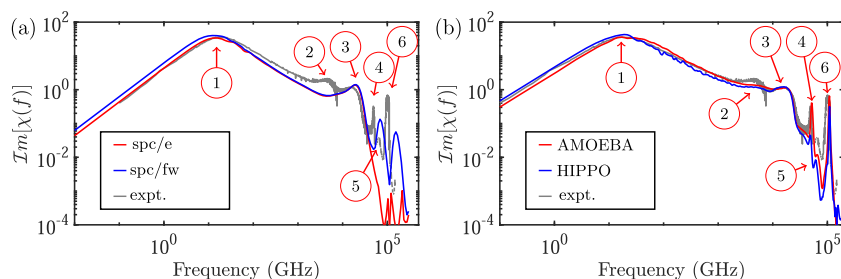


FIG. 1. (a) Imaginary component of spectra determined through our FDT method for SPC/E water (dotted red) and SPC/Fw water (solid red) at 300 K and experimental spectrum from the literature (gray). Peak positions are indicated with the plus signs, and a 95% confidence interval is shaded around each curve. (b) Simulated dielectric spectrum using the AMOEBA03 water model (red) and HIPPO force field (blue) with a composite experimental spectrum (gray) for comparison. Peaks are numbered by relaxation processes described in the text.

the static components dominates. Each spectral component peaks at the same Debye frequency. This suggests that the contribution from the induced polarization is incidental rather than the root cause of the peak. That is, the induced dipoles are aligned with the field as a consequence of the static charges and dipoles being aligned to the field. Furthermore, when the geometry of AMOEBA03 water is kept rigid, it can also reproduce the Debye peak, as can both rigid and flexible non-polarizable models [Fig. 1(a)]. All these reproduce the correct relaxation time (τ_D) of the Debye peak to within 30% error. These taken together mean that the Debye peak of water is an entirely inter-molecular relaxation process.

Conversely, the next-highest frequency peak (Peak 2) is attributable primarily to the induced dipole moment polarization (Fig. 2), as previously observed in AIMD simulations.³² AMOEBA is able to capture the frequency of this peak solely from the induced atomic dipolar interactions, although the magnitude of the simulated peak is lower than the experimental one. However, HIPPO adds additional time-variant multipolar interactions compared to AMOEBA03, yet even further underpredicts the magnitude of this peak. The performance of HIPPO is surprising considering that charge transfer among water molecules contributes to the magnitude of the analogous Raman peak.^{57,65} This shows that the use of a polarizable force field, while necessary to describe the interactions that cause this peak, is not necessarily sufficient depending on the polarizable force field.^{18,65} HIPPO's performance may be because the charge transfer term in HIPPO does not involve explicit transfer of charges. It instead is solely an energetic term rather than an explicit charge distribution term that would impact the dielectric response.

The remaining four peaks in water's dielectric spectrum are closely associated with water's infrared-active modes. Peak three is a libration mode; peak four is an angle-bending mode; peak five is an asymmetric bond stretch; and peak six is a symmetric bond stretch.^{18,32,66,67} The libration is a whole-molecule rocking motion and so does not require flexible molecular geometry for this motion to occur in simulations. Therefore, rigid force fields, such as SPC/E, can reproduce this peak [Fig. 1(a)]. However, all the remaining three peaks require intramolecular motions and so are reproduced only by using flexible models.

Changing temperature

To further resolve water's spectral features, we decompose its spectrum at temperatures ranging from 275 to 350 K, as shown in

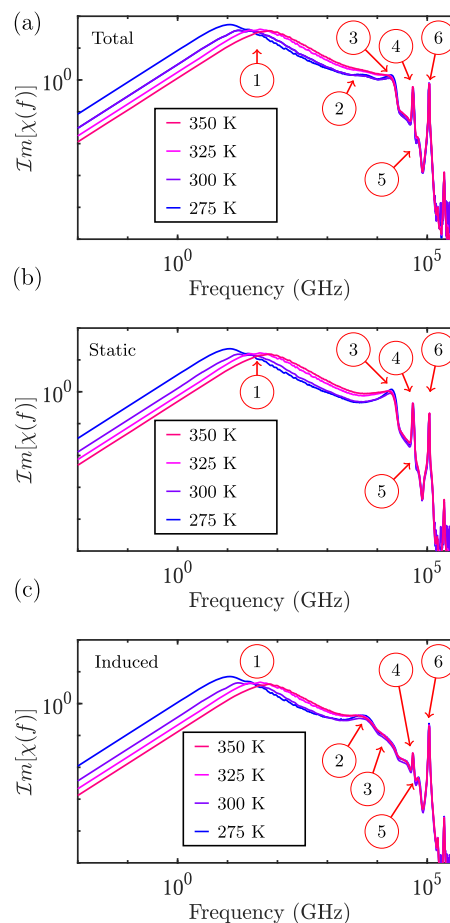


FIG. 3. Total (a), static (b), and induced (c) dielectric spectra of liquid water at temperatures of 350 K (red), 325 K (pink), 300 K (purple), and 275 K (blue).

Fig. 3. Notably, the relative magnitude of the static and induced contributions to each peak appears to be independent of temperature. With decreasing temperature, peak 1 shifts to lower frequencies. The dielectric constant also increases in magnitude with decreasing temperature; see Table SI (supplementary material). The decreasing

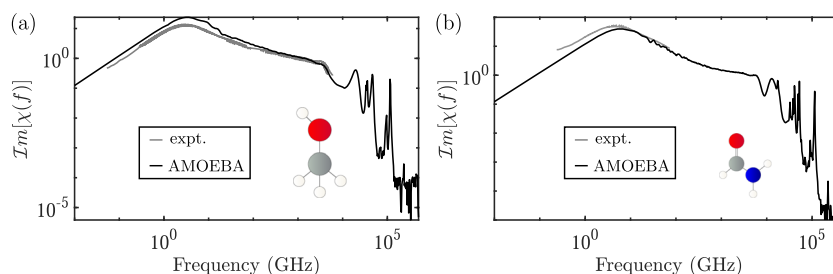


FIG. 4. Total dielectric spectra (black) of (a) methanol and (b) formamide using the AMOEBA09 force field at 300 K compared to experimental spectra (gray) for methanol and formamide.^{53,54} Molecular structures are indicated in the ball-and-stick format.

frequency of peak 1 isolates peak 2, which is particularly clear from the induced spectra [Fig. 3(c)]. Peak 3 becomes sharper at lower temperature, as expected from experimental observations from IR spectroscopy (identified in that reference as peak L_2).⁵⁴ This may be attributed to the (experimentally observed⁵³) stiffening of the hydrogen bonding network with decreasing temperature. The increasing hydrogen bond strength constrains the librating motion and thus narrows the distribution of time scales at which the libration occurs. In contrast to the low frequency peaks resulting from intermolecular motions, the location of the spectral features at higher frequencies are mostly unchanged with temperature, a trend also observed experimentally⁶⁸ in the analogous IR modes.

Other solvents

Demonstrating this approach with other solvents, we calculate the dielectric spectra of methanol and formamide using the AMOEBA09 force field. Figure 4 shows these computed spectra [methanol in panel (a) and formamide in panel (b)] alongside experimental data.^{60–64} The formamide and methanol Debye peaks are at lower frequencies than water's Debye peak, and their spectra contain several peaks over a broad frequency range. The calculated dielectric spectra agree well with the experimental spectra from the literature, further illustrating the utility of both this method and the AMOEBA force field.

CONCLUSIONS

We have developed a new method for computing the dielectric spectrum of solvents through the fluctuation dissipation theorem. We used this to benchmark the AMOEBA03 polarizable water model against several well-known non-polarizable models of water, including force fields with both rigid and flexible geometry. The calculated spectrum from AMOEBA03 reproduces all the spectral features in water's dielectric spectrum, unlike the non-polarizable models. Furthermore, we decomposed the spectra of water at multiple temperatures into components resulting from the static and induced polarizations. Using this decomposition, we identified that one spectral feature, peak 2, is produced purely by induced multipolar interactions, explaining its absence in spectra from non-polarizable force fields. We also demonstrate the use of this method with the AMOEBA09 force field to calculate the dielectric spectra of methanol and formamide, both of which agree well with the experiment.

SUPPLEMENTARY MATERIAL

The [supplementary material](#) contains tables of the dielectric relaxation parameters for water from spectra produced from various force fields and a temperature sweep using the AMOEBA03 water model. Details of the fitting procedure are also provided. An error analysis relating to simulation time is also provided. The Python code to perform our dielectric spectrum determination, along with molecular dynamics input files for each liquid, is provided here. Input parameters for the code to calculate dielectric spectra via our method are explained in the [supplementary material](#).

ACKNOWLEDGMENTS

R.A.B. acknowledges support from the U.S. Department of Commerce, National Institute of Standards and Technology under the financial assistance Award No. 70NANB22H002. J.W.P. and M.K.J.C. acknowledge support from NIH NIGMS Grant No. R01 GM106137 and NIH NIGMS Grant No. R01 114237.

We thank Jennifer Clark and Yasaman Kazempour for their helpful manuscript feedback.

This article was prepared in part by Theiss Research using Federal Funds under Award No. 70NANB22H002 from the National Institute of Standards and Technology, U.S., Department of Commerce. The statements, findings, conclusions, and recommendations are those of the authors and do not necessarily reflect the views of the National Institute of Standards and Technology or the U.S. Department of Commerce.

AUTHOR DECLARATIONS

Conflict of Interest

The authors have no conflicts to disclose.

Author Contributions

Rebecca A. Bone: Conceptualization (equal); Data curation (equal); Formal analysis (equal); Investigation (equal); Methodology (equal); Validation (equal); Writing – original draft (equal); Writing – review & editing (equal). **Moses K.J. Chung:** Investigation (equal); Methodology (equal); Software (equal); Writing – review & editing (equal). **Jay W. Ponder:** Investigation (equal); Methodology (equal); Supervision (equal); Writing – review & editing (equal). **Demian Riccardi:** Formal analysis (equal); Writing – review & editing (equal). **Chris Muzny:** Formal analysis (equal); Project administration (equal); Supervision (equal); Writing – review & editing (equal). **Ravishankar Sundararaman:** Conceptualization (equal); Formal analysis (equal); Software (equal); Writing – review & editing (equal). **Kathleen Schwarz:** Conceptualization (equal); Funding acquisition (equal); Project administration (equal); Resources (equal); Supervision (equal); Writing – original draft (equal); Writing – review & editing (equal).

DATA AVAILABILITY

The data that support the findings of this study are available from the corresponding author upon reasonable request.

REFERENCES

- ¹F. Kremer and A. Schönhal, *Broadband Dielectric Spectroscopy* (Springer, 2003).
- ²R. Buchner, J. Barthel, and J. Stauber, "The dielectric relaxation of water between 0 °C and 35 °C," *Chem. Phys. Lett.* **306**, 57–63 (1999).
- ³N. Penkov, N. Shvirst, V. Yashin, E. Fesenko, Jr, and E. Fesenko, "Terahertz spectroscopy applied for investigation of water structure," *J. Phys. Chem. B* **119**, 12664–12670 (2015).
- ⁴A. Landoulsi, J. Leroy, C. Dalmay, A. Pothier, A. Bessaudou, and P. Blondy, "A microfluidic sensor dedicated to microwave dielectric spectroscopy of liquids medium and flowing colloidal suspension," *Procedia Eng.* **87**, 504–507 (2014), Eurosensors 2014, the 28th European Conference on Solid-State Transducers.

- ⁵A. Erkoreka and J. Martinez-Perdiguerro, "Development of a high-frequency dielectric spectrometer using a portable vector network analyzer," *Rev. Sci. Instrum.* **95**, 023903 (2024).
- ⁶M. Cifra, J. Průša, D. Havelka, and O. Krivosudský, "Molecular dynamics simulations in service of microwave dielectric analysis of biomolecules," in *2018 IEEE International Microwave Biomedical Conference IMBioC* (IEEE, 2018), pp. 28–30.
- ⁷S. Boresch, P. Höchtel, and O. Steinhauser, "Studying the dielectric properties of a protein solution by computer simulation," *J. Phys. Chem. B* **104**, 8743–8752 (2000).
- ⁸Y. N. Kaznessis, D. A. Hill, and E. J. Maginn, "Molecular dynamics simulations of dielectric relaxation of concentrated polymer solutions," *J. Chem. Phys.* **111**, 1325–1334 (1999).
- ⁹J. L. F. Abascal and C. Vega, "A general purpose model for the condensed phases of water: TIP4P/2005," *J. Chem. Phys.* **123**, 234505 (2005).
- ¹⁰N. Kumagai, K. Kawamura, and T. Yokokawa, "An interatomic potential model of H₂O: Applications to water and ice polymorphs," *Mol. Simul.* **12**, 177–186 (1994).
- ¹¹P. Mark and L. Nilsson, "Structure and dynamics of the TIP3P, SPC, and SPC/E water models at 298 K," *J. Phys. Chem. A* **105**, 9954–9960 (2001).
- ¹²K. M. Dyer, J. S. Perkyns, S. George, and B. Montgomery Pettitt, "Site-normalised molecular fluid theory: On the utility of a two-site model of water," *Mol. Phys.* **107**, 423–431 (2009).
- ¹³H. J. C. Berendsen, J. R. Grigera, and T. P. Straatsma, "The missing term in effective pair potentials," *J. Phys. Chem.* **91**, 6269–6271 (1987).
- ¹⁴P. Ren and J. W. Ponder, "Polarizable atomic multipole water model for molecular mechanics simulation," *J. Phys. Chem. B* **107**, 5933–5947 (2003).
- ¹⁵J. W. Ponder, C. Wu, P. Ren, V. S. Pande, J. D. Chodera, M. J. Schnieders, I. Haque, D. L. Mobley, D. S. Lambrecht, R. A. DiStasio, Jr, M. Head-Gordon, G. N. I. Clark, M. E. Johnson, and T. Head-Gordon, "Current status of the AMOEBA polarizable force field," *J. Phys. Chem. B* **114**, 2549–2564 (2010).
- ¹⁶A. Dodin and P. L. Geissler, "Symmetrized drude oscillator force fields improve numerical performance of polarizable molecular dynamics," *J. Chem. Theory Comput.* **19**, 2906–2917 (2023).
- ¹⁷E. Harder, V. M. Anisimov, I. V. Vorobyov, P. E. M. Lopes, S. Y. Noskov, A. D. MacKerell, and B. Roux, "Atomic level anisotropy in the electrostatic modeling of lone pairs for a polarizable force field based on the classical drude oscillator," *J. Chem. Theory Comput.* **2**, 1587–1597 (2006).
- ¹⁸M. Sega and C. Schröder, "Dielectric and terahertz spectroscopy of polarizable and nonpolarizable water models: A comparative study," *J. Phys. Chem. A* **119**, 1539–1547 (2015).
- ¹⁹J. A. Rackers, R. R. Silva, Z. Wang, and J. W. Ponder, "Polarizable water potential derived from a model electron density," *J. Chem. Theory Comput.* **17**, 7056–7084 (2021).
- ²⁰M. L. Berkowitz, "Molecular simulations of aqueous electrolytes: Role of explicit inclusion of charge transfer into force fields," *J. Phys. Chem. B* **125**, 13069–13076 (2021).
- ²¹J. A. Rackers, Q. Wang, C. Liu, J.-P. Piquemal, P. Ren, and J. W. Ponder, "An optimized charge penetration model for use with the AMOEBA force field," *Phys. Chem. Chem. Phys.* **19**, 276–291 (2017).
- ²²R. Chelli, M. Pagliai, P. Procacci, G. I. Cardini, and V. Schettino, "Polarization response of water and methanol investigated by a polarizable force field and density functional theory calculations: Implications for charge transfer," *J. Chem. Phys.* **122**, 074504 (2005).
- ²³D. van der Spoel, P. J. van Maaren, and H. J. C. Berendsen, "A systematic study of water models for molecular simulation: Derivation of water models optimized for use with a reaction field," *J. Chem. Phys.* **108**(24), 10220–10230 (1998).
- ²⁴M. Rami Reddy and M. Berkowitz, "The dielectric constant of SPC/E water," *Chem. Phys. Lett.* **155**(2), 173–176 (1989).
- ²⁵G. Raabe and R. J. Sadus, "Molecular dynamics simulation of the dielectric constant of water: The effect of bond flexibility," *J. Chem. Phys.* **134**, 234501 (2011).
- ²⁶D. Braun, S. Boresch, and O. Steinhauser, "Transport and dielectric properties of water and the influence of coarse-graining: Comparing BMW, SPC/E, and TIP3P models," *J. Chem. Phys.* **140**, 064107 (2014).
- ²⁷M. Woodcox, A. Mahata, A. Hagerstrom, A. Stelson, C. Muzny, R. Sundararaman, and K. Schwarz, "Simulating dielectric spectra: A demonstration of the direct electric field method and a new model for the nonlinear dielectric response," *J. Chem. Phys.* **158**, 124122 (2023).
- ²⁸S. Izadi and A. V. Onufriev, "Accuracy limit of rigid 3-point water models," *J. Chem. Phys.* **145**, 074501 (2016).
- ²⁹Z. Liu, J. Timmermann, K. Reuter, and C. Scheurer, "Benchmarks and dielectric constants for reparametrized OPLS and polarizable force field models of chlorinated hydrocarbons," *J. Phys. Chem. B* **122**, 770–779 (2018).
- ³⁰C. Caleman, P. J. van Maaren, M. Hong, J. S. Hub, L. T. Costa, and D. van der Spoel, "Force field benchmark of organic liquids: Density, enthalpy of vaporization, heat capacities, surface tension, isothermal compressibility, volumetric expansion coefficient, and dielectric constant," *J. Chem. Theory Comput.* **8**, 61–74 (2012).
- ³¹O. Marsalek and T. E. Markland, "Quantum dynamics and spectroscopy of *ab initio* liquid water: The Interplay of nuclear and electronic quantum effects," *J. Phys. Chem. Lett.* **8**, 1545–1551 (2017).
- ³²S. Carlson, F. N. Brüning, P. Loche, D. J. Bonhuis, and R. R. Netz, "Exploring the absorption spectrum of simulated water from MHz to infrared," *J. Phys. Chem. A* **124**, 5599–5605 (2020).
- ³³F. Deisenbeck and S. Wippermann, "Dielectric properties of nanoconfined water from *ab initio* thermopotentiostat molecular dynamics," *J. Chem. Theory Comput.* **19**, 1035–1043 (2023).
- ³⁴V. Dubois, P. Umari, and A. Pasquarello, "Dielectric susceptibility of dipolar molecular liquids by *ab initio* molecular dynamics: Application to liquid HCl," *Chem. Phys. Lett.* **390**, 193–198 (2004).
- ³⁵C. Zhang, J. Hutter, and M. Sprik, "Computing the Kirkwood g-factor by combining constant Maxwell electric field and electric displacement simulations: Application to the dielectric constant of liquid water," *J. Phys. Chem. Lett.* **7**, 2696–2701 (2016).
- ³⁶C. Zhang and M. Sprik, "Computing the dielectric constant of liquid water at constant dielectric displacement," *Phys. Rev. B* **93**, 144201 (2016).
- ³⁷J. H. Ryu, J. W. Yu, T. J. Yoon, and W. B. Lee, "Understanding the dielectric relaxation of liquid water using neural network potential and classical pairwise potential," *J. Mol. Liq.* **397**, 124054 (2024).
- ³⁸S. Chmiela, V. Vassilev-Galindo, O. T. Unke, A. Kabylda, H. E. Sauceda, A. Tkatchenko, and K.-R. Müller, "Accurate global machine learning force fields for molecules with hundreds of atoms," *Sci. Adv.* **9**(2), eadf0873 (2023).
- ³⁹M. Neumann and O. Steinhauser, "On the calculation of the frequency-dependent dielectric constant in computer simulations," *Chem. Phys. Lett.* **102**, 508–513 (1983).
- ⁴⁰S. I. Mamatkulov, K. F. Rinne, R. Buchner, R. R. Netz, and D. J. Bonhuis, "Water-separated ion pairs cause the slow dielectric mode of magnesium sulfate solutions," *J. Chem. Phys.* **148**, 222812 (2018).
- ⁴¹L. Martínez, R. Andrade, E. G. Birgin, and J. M. Martínez, "PACKMOL: A package for building initial configurations for molecular dynamics simulations," *J. Comput. Chem.* **30**, 2157–2164 (2009).
- ⁴²J. A. Rackers, Z. Wang, C. Lu, M. L. Laury, L. Lagardère, M. J. Schnieders, J.-P. Piquemal, P. Ren, and J. W. Ponder, "Tinker 8: Software tools for molecular design," *J. Chem. Theory Comput.* **14**(10), 5273–5289 (2018).
- ⁴³Z. Wang and J. W. Ponder (2022), "Tinker9: Next generation of tinker with GPU support," Dataset <https://github.com/TinkerTools/tinker9>
- ⁴⁴K. F. Rinne, S. Gekle, and R. R. Netz, "Dissecting ion-specific dielectric spectra of sodium-halide solutions into solvation water and ionic contributions," *J. Chem. Phys.* **141**(21), 214502 (2014).
- ⁴⁵V. Balos, P. Müller, G. Jakob, M. Kläui, and M. Sajadi, "Imprinting the complex dielectric permittivity of liquids into the spintronic terahertz emission," *Appl. Phys. Lett.* **119**, 091104 (2021).
- ⁴⁶J. Barthel, K. Bachhuber, R. Buchner, H. Hetzenauer, and M. Kleebauer, "A computer-controlled system of transmission lines for the determination of the complex permittivity of lossy liquids between 8.5 and 90 GHz," *Ber. Bunsenges. Phys. Chem.* **95**, 853–859 (1991).
- ⁴⁷Z. Czumaj, "Absorption coefficient and refractive index measurements of water in the millimetre spectral range," *Mol. Phys.* **69**, 787–790 (1990).
- ⁴⁸D. Downing and D. Williams, "Optical constants of water in the infrared," *J. Geophys. Res.* **80**, 1656–1661 (1975).

- ⁴⁹G. M. Hale and M. R. Querry, "Optical constants of water in the 200-nm to 200- μm wavelength region," *Appl. Opt.* **12**, 555–563 (1973).
- ⁵⁰U. Kaatz, "Complex permittivity of water as a function of frequency and temperature," *J. Chem. Eng. Data* **34**, 371–374 (1989).
- ⁵¹K. Shiraga, Y. Ogawa, and N. Kondo, "Hydrogen bond network of water around protein investigated with terahertz and infrared spectroscopy," *Biophys. J.* **111**, 2629–2641 (2016).
- ⁵²H. P. Schwan, R. J. Sheppard, and E. H. Grant, "Complex permittivity of water at 25 °C," *J. Chem. Phys.* **64**, 2257–2258 (1976).
- ⁵³J. K. Vij, D. R. J. Simpson, and O. E. Panarina, "Far infrared spectroscopy of water at different temperatures: GHz to THz dielectric spectroscopy of water," *J. Mol. Liq.* **112**, 125–135 (2004).
- ⁵⁴H. R. Zelsmann, "Temperature dependence of the optical constants for liquid H₂O and D₂O in the far IR region," *J. Mol. Struct.* **350**, 95–114 (1995).
- ⁵⁵A. Offei-Danso, U. N. Morzan, A. Rodriguez, A. Hassanali, and A. Jelic, "The collective burst mechanism of angular jumps in liquid water," *Nat. Commun.* **14**, 1345 (2023).
- ⁵⁶C. Hölzl, H. Forbert, and D. Marx, "Dielectric relaxation of water: Assessing the impact of localized modes, translational diffusion, and collective dynamics," *Phys. Chem. Chem. Phys.* **23**, 20875 (2021).
- ⁵⁷H. Torii, "Intermolecular electron density modulations in water and their effects on the far-infrared spectral profiles at 6 THz," *J. Phys. Chem. B* **115**, 6636–6643 (2011).
- ⁵⁸N. Mauger, T. Plé, L. Lagardère, S. Huppert, and J. P. Piquemal, "Improving condensed-phase water dynamics with explicit nuclear quantum effects: The polarizable Q-AMOEBa force field," *J. Phys. Chem. B* **126**, 8813–8826 (2022).
- ⁵⁹M. L. Laury, L.-P. Wang, V. S. Pande, T. Head-Gordon, and J. W. Ponder, "Revised parameters for the AMOEBa polarizable atomic multipole water model," *J. Phys. Chem. B* **119**, 9423–9437 (2015).
- ⁶⁰T. Fukasawa, T. Sato, J. Watanabe, Y. Hama, W. Kunz, and R. Buchner, "Relation between dielectric and low-frequency Raman spectra of hydrogen-bonded liquids," *Phys. Rev. Lett.* **95**, 197802 (2005).
- ⁶¹B. P. Jordan, R. J. Sheppard, and S. Szwarnowski, "The dielectric properties of formamide, ethanediol and methanol," *J. Phys. D: Appl. Phys.* **11**(5), 695 (1978).
- ⁶²Y. Yomogida, Y. Sato, R. Nozaki, T. Mishina, and J. Nakahara, "Dielectric study of normal alcohols with THz time-domain spectroscopy," *J. Mol. Liq.* **154**(1), 31–35 (2010).
- ⁶³J. Barthel, K. Bachhuber, R. Buchner, J. B. Gill, and M. Kleebauer, "Dielectric spectra of some common solvents in the microwave region. Dipolar aprotic solvents and amides," *Chem. Phys. Lett.* **167**(1–2), 62–66 (1990).
- ⁶⁴J. Lou, A. K. Paravastu, P. E. Laibinis, and T. A. Hatton, "Effect of temperature on the dielectric relaxation in solvent mixtures at microwave frequencies," *J. Phys. Chem. A* **101**, 9892–9899 (1997).
- ⁶⁵D. Sidler, M. Meuwly, and P. Hamm, "An efficient water force field calibrated against intermolecular THz and Raman spectra," *J. Chem. Phys.* **148**, 244504 (2018).
- ⁶⁶G. E. Walrafen, "Raman spectrum of water: Transverse and longitudinal acoustic modes below $\approx 300\text{ cm}^{-1}$ and optic modes above $\approx 300\text{ cm}^{-1}$," *J. Phys. Chem.* **94**, 2237–2239 (1990).
- ⁶⁷H. Ito and Y. Tanimura, "Simulating two-dimensional infrared-Raman and Raman spectroscopies for intermolecular and intramolecular modes of liquid water," *J. Chem. Phys.* **144**, 074201 (2016).
- ⁶⁸V. S. Langford, A. J. McKinley, and T. I. Quickenden, "Temperature dependence of the visible-near-infrared absorption spectrum of liquid water," *J. Phys. Chem. A* **105**, 8916–8921 (2001).